Neuroanatomical Differences Associated with Stress Susceptibility and Resilience

Supplemental Information

Supplemental Materials and Methods

Aggression Screening

During a three-day screening procedure a novel C57/BL6 mouse was introduced daily into the home cage of a CD1 retired breeder mouse. The latency to attack and the total number of attacks during a 3-min testing session were recorded for each CD1 mouse. Mice that attacked on at least two consecutive days in less than 60 s were included as aggressors. Aggressors were ranked based on their aggression scores (total sum of all attacks/total latency to the first attack). During the social defeat stress procedure, experimental C57/BL6 mice were alternated between CD1 aggressors with low and high aggression scores and the total aggression exposure throughout the 10-day defeat paradigm was maintained at similar levels for each individual.

Perfusions

All mice were perfused 24 h after the social interaction test. Mice were anesthetized with sodium pentobarbital and perfused with 30 ml PBS containing Heparin (1 µl/ml) and ProHance contrast reagent (2 mM; Bracco, Montreal, CA), followed by 30 ml of 4% PFA containing Heparin (1 µl/ml) and ProHance contrast reagent (2 mM) at a flow rate of 1.0 ml/min. Brains remained in the skull to avoid deformations and damage during removal. Brains were post-fixed over night at 4°C in 4% PFA + ProHance solution (2 mM) (1).

Image Analysis

Brains were aligned using nonlinear image registration with iterative template refinement encapsulated into a custom pipeline (2-4) using the ANTS registration algorithm (5,6). Input images were rigidly registered to a pre-defined template and averaged to create a new template. An improved template was generated at each iteration by further relaxing the constraints on the registration. Template refinement was stopped after three successively non-linear registration steps. The log-transformed Jacobian determinants of the final transformation fields (log-Jacobians) for each brain were smoothed using a Gaussian kernel (0.2 mm FWHM). The Jacobian determinants represent the volume ratio of the original versus the transformed image at each voxel, i.e., local volume increases or decreases. Pre-made atlases were registered to the final non-linear average (7-10) to determine the volume of specific anatomical regions and for analysis of local volume differences within *a priori* regions-of-interest (ROI). The volume of each anatomical region in each individual was obtained by inverting the final non-linear registration and projecting the atlas onto each individual brain. Atlas regions were corrected manually to account for registration errors. Cingulate area 32 and medial orbitofrontal cortex were joined into ROI 'cingulate cortex' and nucleus accumbens and basal forebrain were joined into ROI 'nucleus accumbens'. For the *a priori* selected brain regions in the atlas-based comparisons of group-level structural differences between susceptible and resilient mice (Figure S4, Tables S1, S2), we present effect sizes (Cohen’s d) and uncorrected *p*-values.

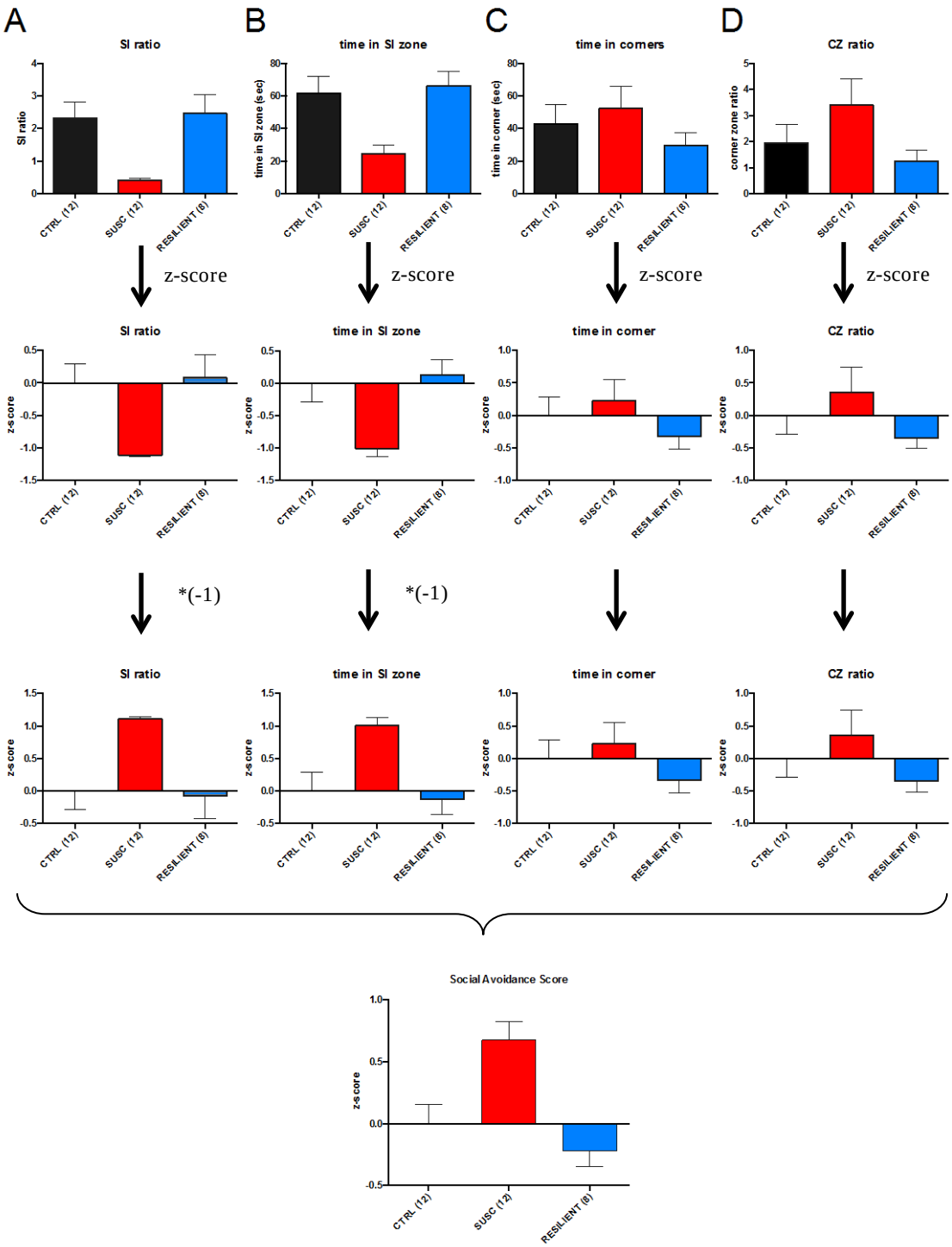

Figure S1. Computation of social avoidance z-score based on behavior in the social interaction test. (**A**) Social interaction ratios for control and defeated mice. Defeated mice are divided into susceptible and resilient groups based on their social interaction (SI) ratio (>1 = resilient; <1 = susceptible). (**B**) Time in social interaction zone, (**C**) time in corner zones, and (**D**) corner zone ratios. Z-scores are calculated for each behavioral outcome. SI ratios and time spent in SI zone are multiplied by -1, so that higher z-scores reflect more social avoidance. The average of all four z-scores is used as the social avoidance score.

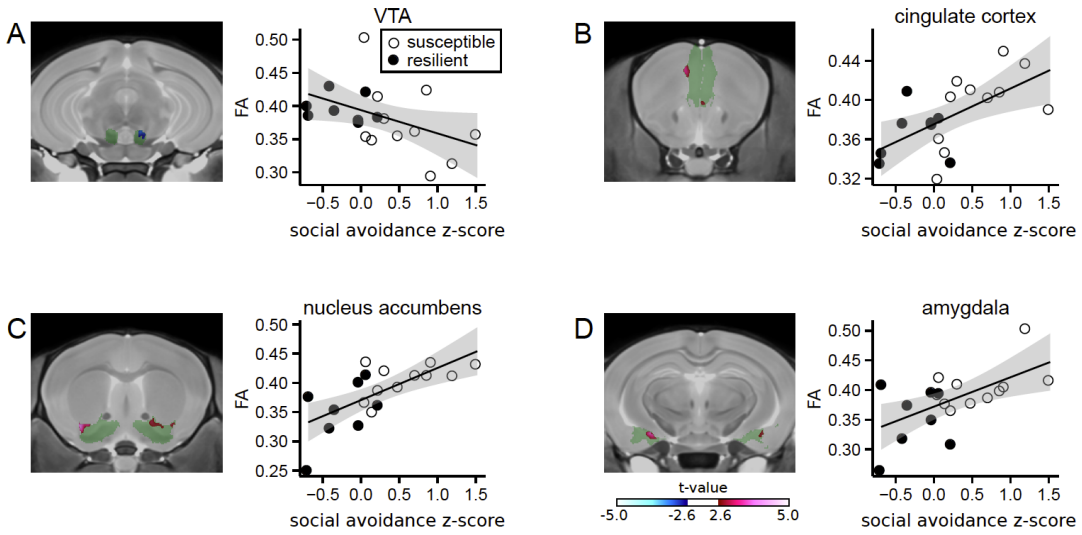

Figure S2. Correlations between social avoidance and fractional anisotropy (FA) of previously established stress-related brain structures. Social avoidance z-scores are correlated with FA at the most significant voxel within selected brain structures. (**A**) Negative correlation with ventral tegmental area, (**B**) positive correlation with cingulate cortex, (**C**) positive correlation with nucleus accumbens, and (**D**) positive correlation with amygdala. Areas shaded in green indicate the entire brain structure, blue and red areas indicate regions with significant volume changes. Clear circles: susceptible mice (*n* = 11), black circles: resilient mice (*n* = 8) based on social interaction ratio.

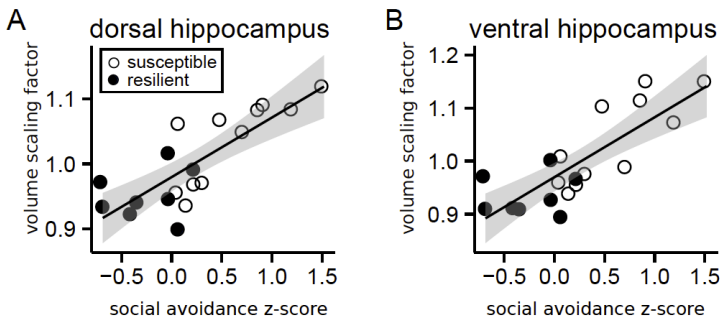

Figure S3. Correlations between social avoidance and volumes of dorsal and ventral hippocampus. (**A**) Positive correlation between social avoidance score and dorsal hippocampus, and (**B**) positive correlation between social avoidance score and ventral hippocampus. Clear circles: susceptible mice (*n* = 11), black circles: resilient mice (*n* = 8) based on social interaction ratio.

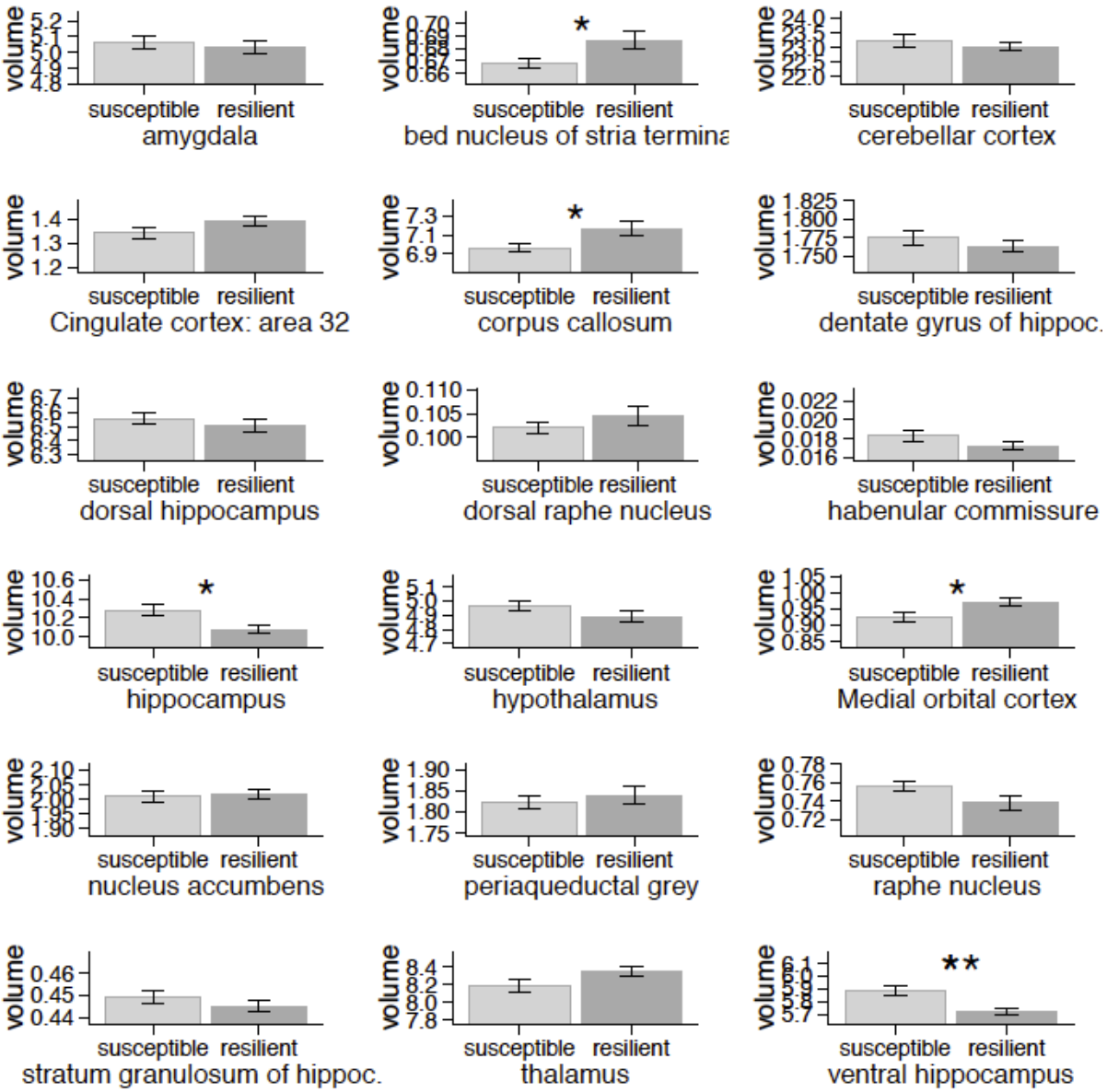

Figure S4. Atlas-based comparisons of group-level structural differences in susceptible (n = 11) and resilient mice (n = 8), which are also shown in Tables S1 and S2. *p < 0.05, **p < 0.01.

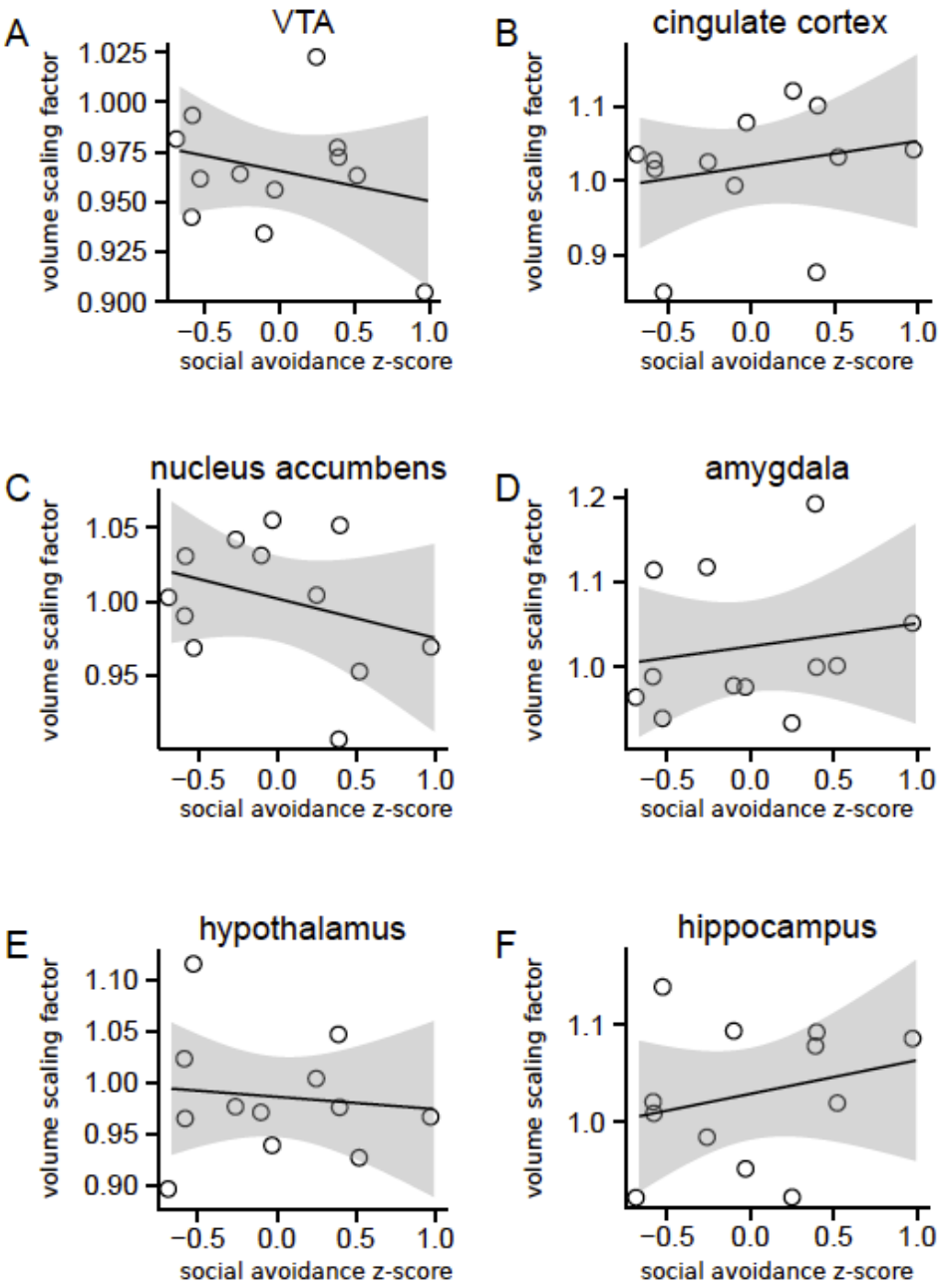

Figure S5. Correlations between social avoidance and volumes of previously established stress-related brain structures in control animals. No significant correlations are observed between social avoidance z-scores and anatomical volume at the most significant voxel within (**A**) ventral tegmental area, (**B**) cingulate cortex, (**C**) nucleus accumbens, (**D**) amygdala, (**E**) hypothalamus, and (**F**) hippocampus. *n* = 12.

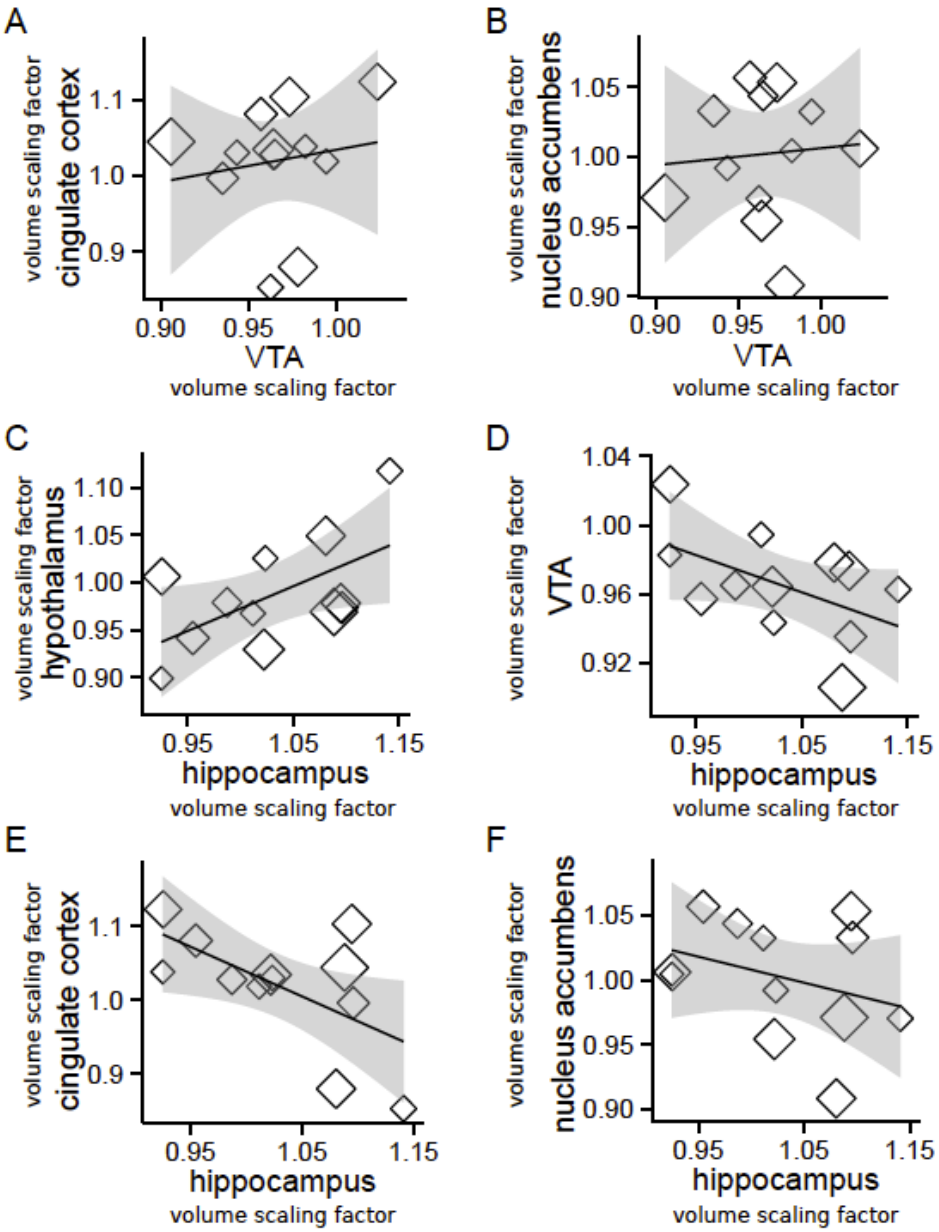

Figure S6. Structural covariance between candidate brain regions in controls. Figure showing peak voxel volume correlations for (**A**) ventral tegmental area and cingulate cortex, (**B**) ventral tegmental area and nucleus accumbens, (**C**) hippocampus and hypothalamus, (**D**) hippocampus and ventral tegmental area, (**E**) hippocampus and cingulate cortex, and (**F**) hippocampus and nucleus accumbens. Square size corresponds to the social avoidance score of the respective animal. *n* = 12.

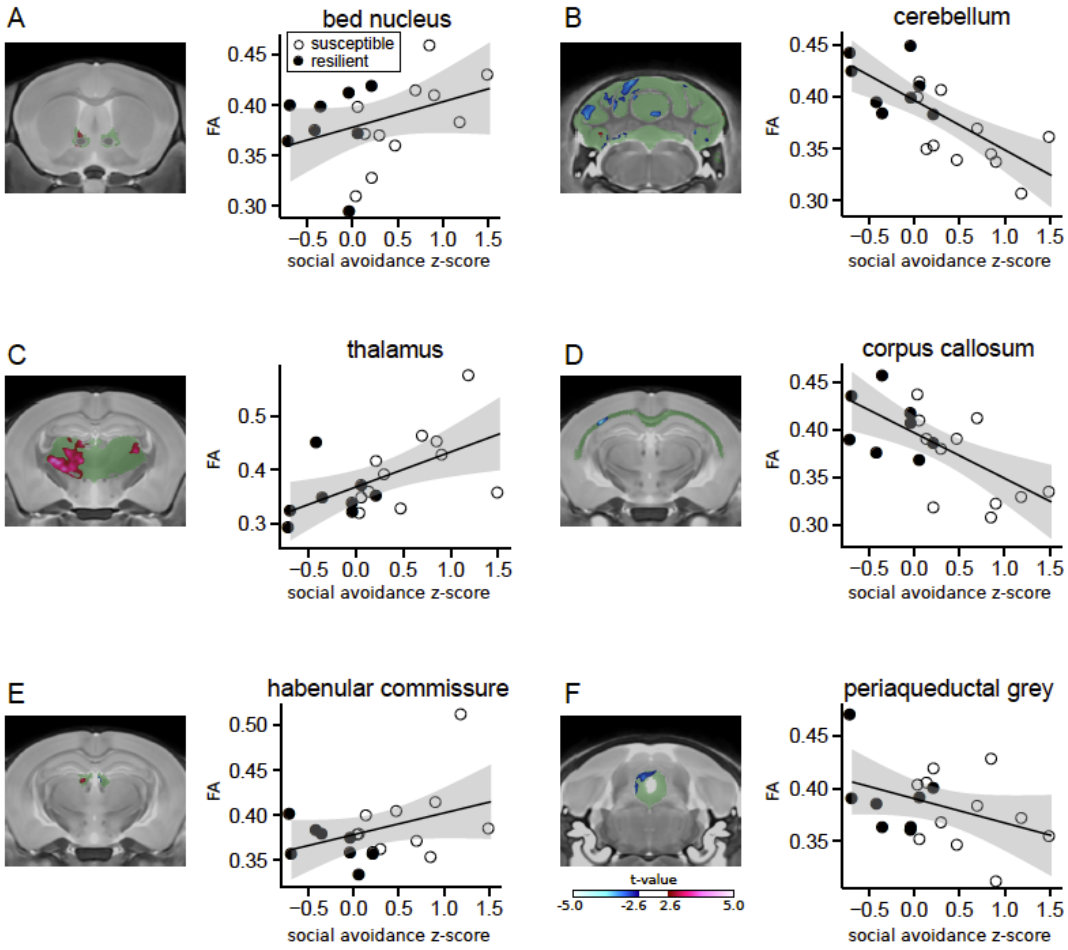

Figure S7. Correlations between social avoidance and fractional anisotropy (FA) of structures not previously associated with social defeat stress. Social avoidance z-scores are correlated with FA at the most significant voxel. **A**) Positive correlation with the bed nucleus of the stria terminals, (**B**) negative correlation with cerebellum, (**C**) positive correlation with thalamus, (**D**) negative correlation with corpus callosum, (**E**) habenular commissure, and (**F**) periaqueductal grey. Areas shaded in green indicate the entire brain structure, blue and red areas indicate regions with significant volume changes. Clear circles: susceptible mice (*n* = 11), black circles: resilient mice (*n* = 8) based on social interaction ratio.

Table S1. Atlas-based comparisons of group-level structural differences between susceptible and resilient mice. Positive effect sizes indicate larger volumes in resilient mice.

Region of Interest (ROI)	*p*-Value	Cohen's d
Ventral Tegmental Area	$p = 0.326$	0.35
Nucleus Accumbens	$p = 0.840$	0.07
Cingulate Cortex: Area 32	$p = 0.129$	0.51
Medial Orbital Cortex	$*p = 0.038$	0.73
Amygdala	$p = 0.583$	-0.18
Hippocampus	$*p = 0.018$	-0.84
Ventral Hippocampus	$**p = 0.005$	-1.02
Dorsal Hippocampus	$p = 0.391$	-0.29
Dentate Gyrus of Hippocampus	$p = 0.354$	-0.30
Stratum Granulosum of Hippocampus	$p = 0.293$	-0.35
Hypothalamus	$p = 0.180$	-0.46

$*p < 0.05$, $**p < 0.01$, uncorrected.

Table S2. Atlas-based comparisons of group-level structural differences between susceptible and resilient mice for novel brain regions. Positive effect sizes indicate larger volumes in resilient mice.

Region of Interest (ROI)	*p*-Value	Cohen's d
Bed Nucleus of Stria Terminalis	**p* = 0.049	0.75
Raphe Nucleus	*p* = 0.076	-0.64
Thalamus	*p* = 0.084	0.58
Corpus Callosum	**p* = 0.031	0.82
Habenular Commissure	*p* = 0.140	-0.49
Periaqueductal Grey	*p* = 0.558	0.2
Cerebellar Cortex	*p* = 0.412	-0.26

**p* < 0.05, uncorrected.

Table S3. Table listing group interactions of group-dependences for all structure-structure correlations shown in Figure 4.

Structure	Est	*p*
VTA - Nucleus Accumbens	0.79	0.12
VTA - Cingulate Cortex	0.28	0.7
VTA - Hippocampus	0.1	0.77
Hippocampus - Hypothalamus	0.23	0.63
Hippocampus - Nucleus Accumbens	0.21	0.59
Hippocampus - Cingulate Cortex	0.29	0.59

Supplemental References

1. Cahill LS, Laliberté CL, Ellegood J, Spring S, Gleave JA, Eede MC, et al. (2012): Preparation of fixed mouse brains for MRI. *Neuroimage*. 60:933-939.
2. Lerch JP, Sled JG, Henkelman RM (2011): MRI phenotyping of genetically altered mice. *Methods Mol Biol*. 711:349-361.
3. Lerch JP, Yiu AP, Martinez-Canabal A, Pekar T, Bohbot VD, Frankland PW, et al. (2011): Maze training in mice induces MRI-detectable brain shape changes specific to the type of learning. *Neuroimage*. 54:2086-2095.
4. Kovacević N, Henderson JT, Chan E, Lifshitz N, Bishop J, Evans AC, et al. (2005): A three-dimensional MRI atlas of the mouse brain with estimates of the average and variability. *Cereb Cortex*. 15:639-645.
5. Avants BB, Tustison NJ, Song G, Cook PA, Klein A, Gee JC (2011): A reproducible evaluation of ANTs similarity metric performance in brain image registration. *Neuroimage*. 54:2033-2044.
6. Avants BB, Tustison NJ, Wu J, Cook PA, Gee JC (2011): An open source multivariate framework for n-tissue segmentation with evaluation on public data. *Neuroinformatics*. 9:381-400.
7. Dorr AE, Lerch JP, Spring S, Kabani N, Henkelman RM (2008): High resolution three-dimensional brain atlas using an average magnetic resonance image of 40 adult C57Bl/6J mice. *Neuroimage*. 42:60-69.
8. Steadman PE, Ellegood J, Szulc KU, Turnbull DH, Joyner AL, Henkelman RM, et al. (2014): Genetic effects on cerebellar structure across mouse models of autism using a magnetic resonance imaging atlas. *Autism Res*. 7:124-137.
9. Ullmann JF, Watson C, Janke AL, Kurniawan ND, Reutens DC (2013): A segmentation protocol and MRI atlas of the C57BL/6J mouse neocortex. *Neuroimage*. 78:196-203.
10. Lein ES, Hawrylycz MJ, Ao N, Ayres M, Bensinger A, Bernard A, et al. (2007): Genome-wide atlas of gene expression in the adult mouse brain. *Nature*. 445:168-176.